Angiography and optical coherence tomography derived shear stress: are they equivalent in my opinion?

Poon, E.K.W.; Wu, X.L.; Dijkstra, J.; O'Leary, N.; Torii, R.; Reiber, J.H.C.; ... ; Serruys, P.W.

The International Journal of Cardiovascular Imaging (2023) 39:1953–1961
https://doi.org/10.1007/s10554-023-02949-0

ORIGINAL PAPER

Angiography and optical coherence tomography derived shear stress: are they equivalent in my opinion?

Eric K. W. Poon[1] · Xinlei Wu[2,3] · Jouke Dijkstra[4] · Neil O'Leary[2] · Ryo Torii[5] · Johan H. C. Reiber[4] · Christos V. Bourantas[6,7] · Peter Barlis[1] · Yoshinobu Onuma[2] · Patrick W. Serruys[2,8,9,10]

Received: 24 February 2023 / Accepted: 31 August 2023 / Published online: 21 September 2023

Abstract
Advances in image reconstruction using either single or multimodality imaging data provide increasingly accurate three-dimensional (3D) patient's arterial models for shear stress evaluation using computational fluid dynamics (CFD). We aim to evaluate the impacts on endothelial shear stress (ESS) derived from a simple image reconstruction using 3D-quantitative coronary angiography (3D-QCA) *versus* a multimodality reconstruction method using optical coherence tomography (OCT) in patients' vessels treated with bioresorbable scaffolds. Seven vessels at baseline and five-year follow-up of seven patients from a previous CFD investigation were retrospectively selected for a head-to-head comparison of angiography-derived *versus* OCT-derived ESS. 3D-QCA significantly underestimated the minimum stent area [MSA] (-2.38mm^2) and the stent length (-1.46 mm) compared to OCT-fusion method reconstructions. After carefully co-registering the region of interest for all cases with a sophisticated statistical method, the difference in MSA measurements as well as the inability of angiography to visualise the strut footprint in the lumen surface have translated to higher angiography-derived ESS than OCT-derived ESS (1.76 Pa or 1.52 times for the overlapping segment). The difference in ESS widened with a more restricted region of interest (1.97 Pa or 1.63 times within the scaffold segment). Angiography and OCT offer two distinctive methods of ESS calculation. Angiography-derived ESS tends to overestimate the ESS compared to OCT-derived ESS. Further investigations into ESS analysis resolution play a vital role in adopting OCT-derived ESS.

Keywords Coronary angiography · Optical coherence tomography · 3D reconstruction · Computational fluid dynamics · Endothelial shear stress

Introduction

Three-dimensional (3D) quantitative measurements of vascular morphology are an important milestone in the diagnosis of the extent and severity of cardiovascular disease (CVD) [1]. Conventional coronary angiography depicts the severity of coronary stenosis in two-dimensional (2D) planes. It allows for quantitative measurements of the stenosis severity (such as diameter and length) with 2D quantitative coronary angiography (2D-QCA), but it fails to

✉ Patrick W. Serruys
patrick.w.j.c.serruys@gmail.com

[1] Department of Medicine, St Vincent's Hospital, Melbourne Medical School, University of Melbourne, Victoria, Australia

[2] Department of Cardiology, University of Galway, Galway, Ireland

[3] Department of Cardiology, The Second Affiliated Hospital, Yuying Children's Hospital of Wenzhou Medical University, Zhejiang, China

[4] Department of Radiology, Leiden University Medical Center, Leiden, The Netherlands

[5] Department of Mechanical Engineering, University College London, London, UK

[6] Device and Innovation Centre, William Harvey Research Institute, Queen Mary University of London, London, UK

[7] Department of Cardiology, Barts Heart Centre, London, UK

[8] Emeritus Professor of Medicine, Erasmus University, Rotterdam, The Netherlands

[9] CÚRAM, SFI Research Centre for Medical Devices, Galway, Ireland

[10] School of Engineering, University of Melbourne, Melbourne, Australia

truly appreciate the 3D complexity of the stenosis along the arterial path. 3D-QCA uses two angiographic projections to reconstruct a model of the coronary artery. Hence, 3D-QCA allows more accurate coronary anatomy delineation than conventional 2D-QCA [1]. One drawback of 3D-QCA is that it approximates a circular or oval lumen created from measurements on the two angiographic projections [2, 3]. This drawback, however, can be overcome by using a hybrid approach that fuses intravascular imaging data (such as intravascular ultrasound [IVUS] or optical coherence tomography [OCT]) with 3D-QCA. This hybrid approach replaces the circular or oval lumen models derived by 3D-QCA with the actual lumen border from IVUS or OCT along the 3D path of the vessel for an accurate representation of the artery [4].

Over the past decades, continuous research effort has been put into advancing the fusion reconstruction approach, allowing an improved and reliable reconstruction of arteries [5]. For example, lumen with local irregularities such as stents [6], plaque rupture and erosion [7, 8], endoluminal flaps [9], etc. Detailed comparison between 3D-QCA and fusion approach-derived haemodynamic variables (such as endothelial shear stress) remains limited. Recent studies compared 3D reconstruction between 3D-QCA, 3D-IVUS and 3D-OCT had demonstrated excellent agreement in both vessel reconstructions and comparable endothelial shear stress (ESS) measurements [10, 11]. Similar findings were reported in minipig coronary artery reconstructions with 3D-QCA and OCT fusion reconstructions, where 3D-QCA has a similar spatial distribution of time-averaged wall shear stress to OCT fusion method [12]. However, these studies were limited to 3D lumen reconstructions of native arteries.

To our best knowledge, this study represents the first investigation comparing *in-vivo* angiography versus OCT-derived ESS in both native and scaffolded segments simultaneously. To investigate that, we reconstructed 7 patients' arteries implanted with a first-generation bioresorbable scaffold using standalone 3D-QCA and an established 3D-OCT fusion reconstruction method. Simultaneous reconstruction of both native and scaffold segments is essential to natural blood flow development over local stent struts and a comprehensive blood flow analysis. Lastly, the effects of post-CFD analysis resolution between angiography versus OCT-derived ESS were systematically studied using sophisticated statistical models.

Materials and methods

Study design and patient selections

Patients implanted with ABSORB Bioresorbable Vascular Scaffold (BVS, Abbott Vascular, Santa Clara, CA, USA) from a previous CFD investigation of OCT-derived ESS were retrospectively selected for angiography-derived ESS analyses. All patients had coronary angiography and OCT immediately after scaffold implantation (baseline) and at five years follow-up. The original study design, protocol and CFD investigations have been previously described [13, 14].

Three-dimensional QCA and OCT fusion method

All seven 3D-OCT models from a previous CFD study were retrospectively analysed [14]. These seven cases have minimum foreshortening and vessel overlapping by angiogram and clear lumen borders by OCT at both baseline and 5-year follow-up as reviewed by an OCT imaging expert.

Angiography was performed as previously described [13]. 3D-QCA models of the studied vessels at both baseline and five-year follow-up were reconstructed with Medis QAngio XA (Medis Medical Imaging, Leiden, the Netherlands). Figure 1 demonstrates a brief summary of 3D-QCA and 3D-OCT fusion reconstruction methods. Two end-diastolic angiographic projections separated by an angle of at least 25° from each other were selected for reconstruction. Anatomic landmarks (e.g. bifurcations) and stent metallic markers were used to segment the region of interest. All 3D-QCA models included the main vessel (vessel of interest) and a side branch > 1 mm in diameter. The side branch helped identify the absolute orientation of the OCT images. Only the main vessel was used for CFD analysis.

A well-established fusion approach was used to combine OCT imaging data to the corresponding 3D centreline and reconstruct the 3D-OCT fusion model (Fig. 1). In brief, OCT frames were co-registered using anatomic landmarks, such as side branch and the stent metallic markers. The delineated OCT lumen contours (QCU-CMS, Leiden, the Netherlands) were placed perpendicularly to 3D-QCA centrelines at their corresponding locations, replacing the approximated elliptical cross-sections of 3D-QCA. The absolute orientation of the OCT lumen borders was first corrected with the corresponding 3D-QCA side branch direction. OCT frame-by-frame twisting along the 3D centreline was adjusted with the sequential triangulation algorithm.

Scaffold's platinum markers (both proximal and distal) were used to differentiate native *versus* scaffolded segments in both 3D-QCA and 3D-OCT fusion models for quantitative measurements (e.g., minimum stent area [MSA], scaffold length, etc.).

Angiography and optical coherence tomography-derived endothelial shear stress

CFD analysis was carried out on each 3D-QCA reconstruction using an in-house developed solver with an extension for

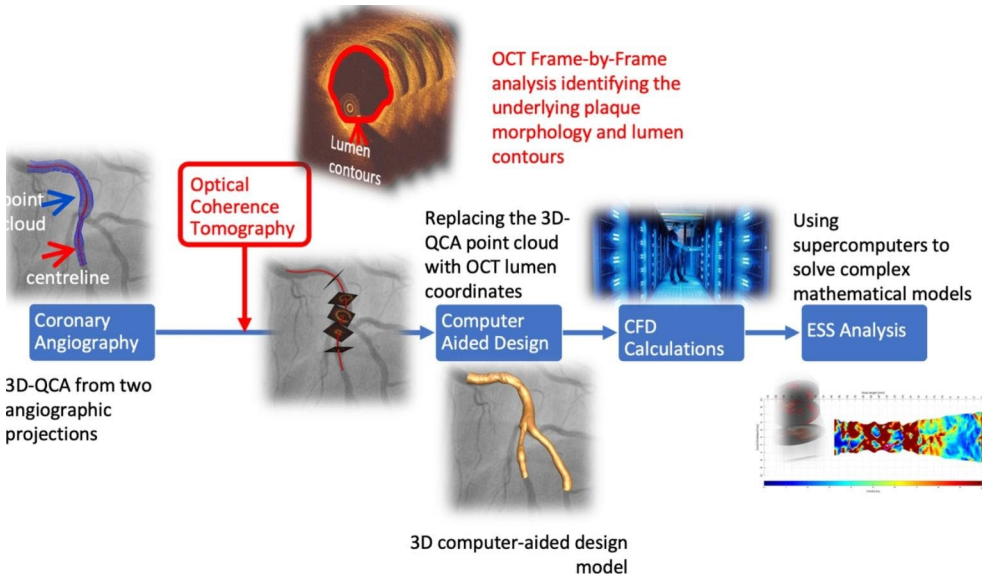

Fig. 1 Endothelial shear stress analysis workflow. In angiography-derived ESS, two angiographic projections that were > 25º apart were used to delineate the lumen border and create the circle or oval lumen shape along a 3D centreline, forming a set of 3D coordinates (point cloud). This point cloud was reconstructed into a water-tight 3D computer-aided design model (blue arrow pathway). The 3D computer-aided design model was divided into thousands to millions of finite-volume elements following the expert recommendations [36]. Blood velocity and pressure were calculated by solving the Navier-Stokes equations on each finite volume element. Finally, the endothelial shear stress was obtained as a product of local blood viscosity and velocity gradient near the lumen surface. The endothelial shear stress on the 3D lumen was transformed into a 2D map with various resolutions for analysis. In OCT-derived ESS, the only difference is that an option pathway (red arrow) was introduced between the point cloud and the water-tight 3D computer-aided design model. In this intermediate step, the previously assumed circle or oval lumen shape was replaced by the actual lumen contours segmented from the OCT images. As a result, a new water-tight 3D computer-aided design model was reconstructed and used for ESS analysis

a non-Newtonian viscosity model based on the open-source CFD package OpenFOAM (v7, The OpenFOAM Foundation Ltd., London, UK) [15]. All simulations followed the exact initial setup and boundary conditions described in [14]. Pulsatile flow simulations were conducted assuming a mean flow rate of ~ 78 ml/s [16]. A non-Newtonian model was applied to mimic the shear-dependent blood rheology [17, 18]. ESS was calculated as the product of near-wall local blood viscosity and the velocity gradient normal to the lumen surface. ESS was reported as the time-averaged shear stress magnitude over the third cardiac cycle. All 14 3D-QCA and their corresponding 3D-OCT fusion models were unfolded to create a two-dimensional (2D) flattened view of the lumen surface with a spatial resolution of 0.2 mm × 1°. These 2D flattened views were co-registered in longitudinal and circumference directions using scaffold platinum markers and anatomical landmarks (e.g., side branches).

Statistical analyses

Statistical analyses were carried out using R-programming language (R Foundation for Statistical Computing Platform v4.02, Vienna, Austria) and MATLAB (The MathWorks Inc., Natick, MA, USA). Continuous variables were summarised with medians (interquartile range [IQR]). Data were summarised and plotted at patient, frame and grid-point levels. All tests were two-tailed with an α-level of 0.05 to indicate statistical significance.

Passing and Bablok regression and Bland-Altman analyses were applied to assess the geometrical agreement (e.g., MSA, scaffold length, etc.) of each 3D-QCA and 3D-OCT fusion model [19]. To compare the difference between angiography-derived *versus* OCT-derived ESS (i.e., shear stress derived from 3D-QCA *versus* 3D-OCT, respectively), all shear stress maps were first transformed from the origin of the arterial direction to the scaffold mid-point (Fig. 2). And to account for the difference in arterial length between 3D-QCA and 3D-OCT fusion models, each arterial model (3D-QCA and 3D-OCT fusion) was normalised by their respective scaffold lengths (Fig. 3). In other words, all axial coordinates have been standardised such that the scaffolded segment covers the axial range [-0.5, 0.5] for every reconstruction. Linear mixed-effects models of ESS were used to evaluate the parameter of primary interest regarding the model reconstruction technique (3D-QCA *versus* 3D-OCT fusion). Other fixed-effects variables were included to control for time point (baseline and follow-up), section type (proximal native, scaffolded, distal native) and a curvilinear change of ESS axially across the vessel. Random-intercept

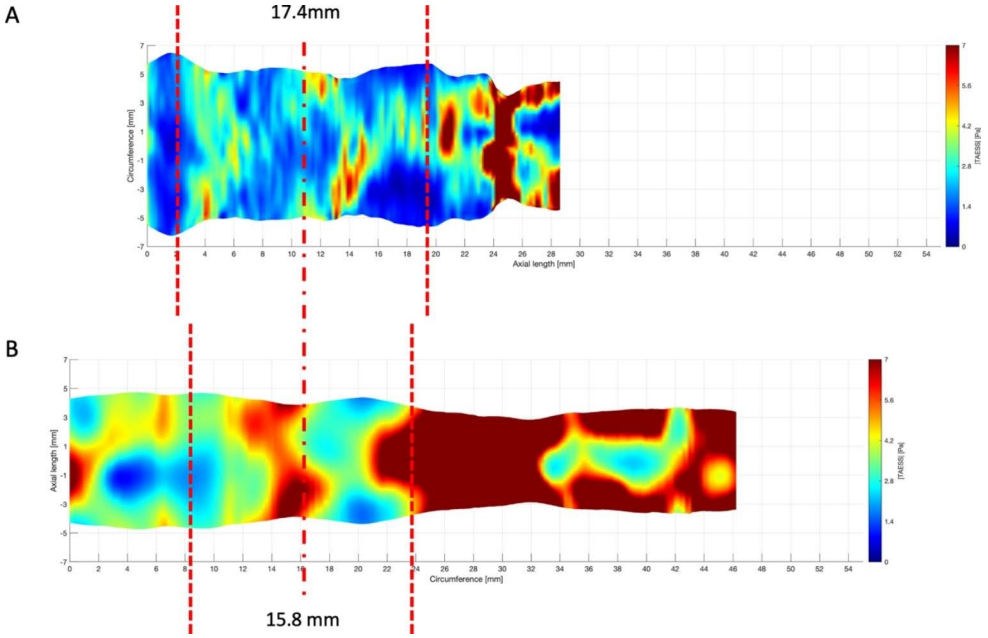

Fig. 2 General representations of the angiography-derived versus OCT-derive ESS. **(A)** OCT-derived ESS and **(B)** Angiography-derived ESS. The 2D ESS map shows the ESS pattern when the artery was cut-open and flattened into a 2D surface with a spatial resolution of 0.2 mm × 1°. The vertical axis represents the local circumference of the lumen, and the horizontal axis is the length of the lumen. The red dashed lines identify the proximal and distal locations of the ABSORB platinum markers. The red dash-dotted line is the mid-distance from both markers

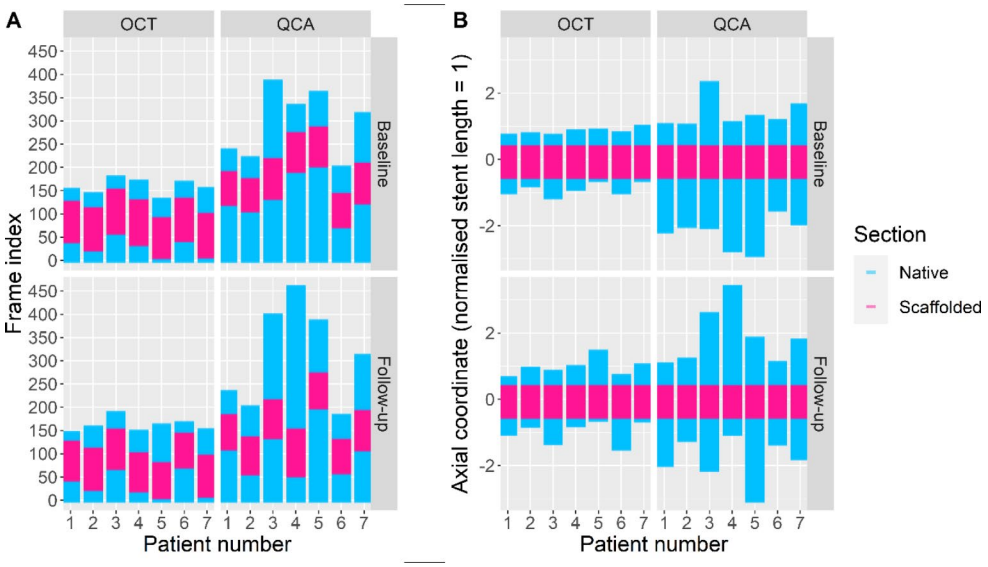

Fig. 3 ESS sampled points. **(A)** raw coordinates and **(B)** scaled to scaffolded section length and transformed to the midpoint. Data points by frame index, patient, segment and image modality

terms were included for patient and segment nested within patient. Comparisons were carried out using:

1) all the data available,
2) on the overlapping segments, including only ESS data where 3D-QCA and 3D-OCT sections are overlapping (according to standardised axial coordinates) for a given reconstruction of a given patient at a given time/visit,
3) including only ESS data within 0.5 stent length of the distal or proximal end of the stent (i.e., all data points with a standardised axial coordinate within the range [-1, 1]), and.
4) the scaffolded segment (within a standardised axial coordinate of [-0.5, 0.5]) only.

A set of sensitivity analyses was conducted where the previously described set of linear, mixed-effects model analyses was replicated but instead using a log-transformed ESS as the response variable. This would assess the impact of different assumptions about ESS distribution (conditionally normal vs. conditionally log-normal) on conclusions and provide parameter estimates comparing the ESS between both methods as a relative difference (ratio) rather than an absolute difference.

Finally, the above linear, mixed-effects model specification was expanded such that all angiography-derived and OCT-derived ESS data were modelled with a separate spline function for each modality (the difference between modes could vary as a function of axial coordinate), and which also

Table 1 Basic study characteristics

	n = 7 (7 vessels from 7 patients at 2 time points)		
Age (years)	62 ± 9		
Male	4(57)		
Treated Vessel			
Left anterior descending	5(71)		
Left circumflex	1(14)		
Right Coronary	1(14)		
Scaffold dimension			
Diameter (mm)	3.00 ± 0.0		
Length (mm)	18.0 ± 0.0		
Nominal scaffold area (mm^2)	7.07 ± 0.0		
Expected scaffold area (mm^2)	8.37 ± 0.53		
	3D-QCA	**3D-OCT**	**p-value**
Measured scaffold dimension			
Length (mm)	16.97 ± 1.69	18.43 ± 1.28	0.014
Minimum scaffold area (mm^2)	3.74 ± 1.14	6.12 ± 1.14	< 0.001
Computational fluid dynamics			
Mesh elements ($\times 10^3$)	91 ± 50	1210 ± 871	< 0.001
Inflow area (mm^2)	6.48 ± 1.25	7.33 ± 1.62	0.12
Blood velocity (mm/s)	0.21 ± 0.04	0.19 ± 0.05	0.17

Values are mean ± standard deviation or n(%)

allowed for discontinuity in the ESS at the scaffolded segment boundary along the vessel (with axial position). The expected ESS values for each modality were estimated in each segment and across the range of standardised axial locations from − 1 to + 1 and these values were plotted.

Results

All seven vessels from seven patients who underwent percutaneous coronary intervention with the ABSORB coronary scaffold and fitted the selection criteria of a previous CFD investigation were included [14]. Table 1 summarises the baseline demographics of the studied patients and the characteristics of the treated vessels.

Figures 4 and 5 illustrate the comparison of the minimum scaffold area (MSA) and scaffold length between 3D-QCA and 3D-OCT fusion methods. The relationship between 3D-QCA and 3D-OCT was weak for these parameters with no evidence of a linear relationship ($r^2 = 0.22$, $p = 0.09$; $r^2 = 0.04$, $p = 0.518$, respectively), albeit this should be interpreted in the context of the small sample size (Fig. 4 A). 3D-QCA consistently underestimated the MSA with a bias of -2.38 mm^2 compared to 3D-OCT (Fig. 4B). Similarly, 3D-QCA underestimated the scaffold length with a bias of -1.46 mm (Fig. 5B). The 95% limits of agreement between 3D-QCA and 3D-OCT methods were also quite wide for both parameters (5.2mm^2 for MSA and 8.5 mm for stent length).

Estimates from the described linear and log-linear mixed effect models of ESS to assess differences in angiography-derived and OCT-derived ESS are displayed in Table 2. Based on these fitted models, we estimated that the average angiography-derived ESS would be higher than the average OCT-derived ESS in a given segment and for a given patient. For example, when considering the difference in ESS on the overlapping sections, the expected angiography-derived ESS is 1.76 Pa higher than the expected OCT-derived ESS; in relative terms, the expected angiography-derived ESS is 1.52 times larger than the expected OCT-derived ESS. The mean difference and the ratio decreased slightly with the

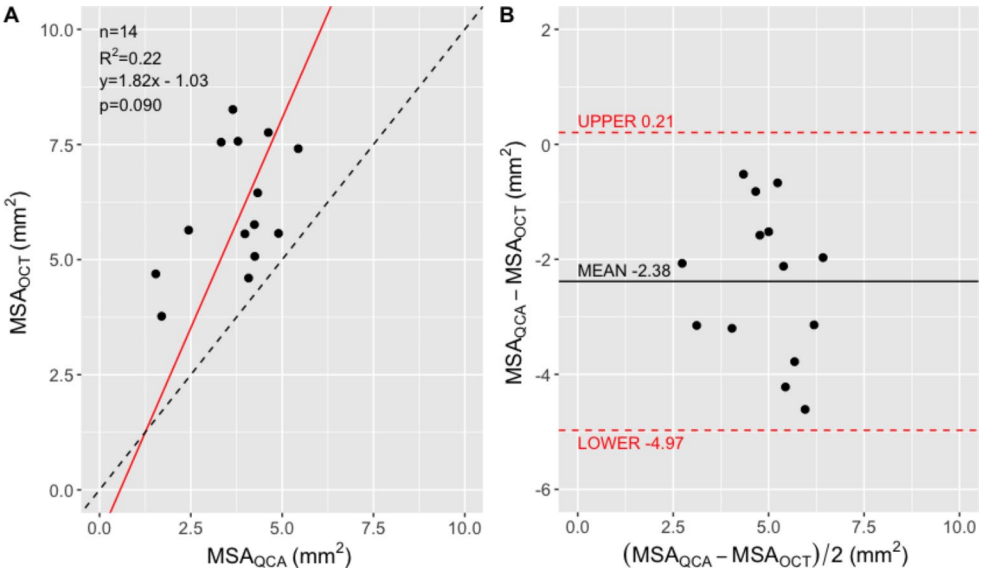

Fig. 4 Minimum stent area measured from 3D-QCA and 3D-OCT fusion method. **(A)** Passing and Bablok regression and **(B)** Bland-Altman analyses. MSA – minimum stent area; QCA – quantitative coronary angiography; OCT – optical coherence tomography

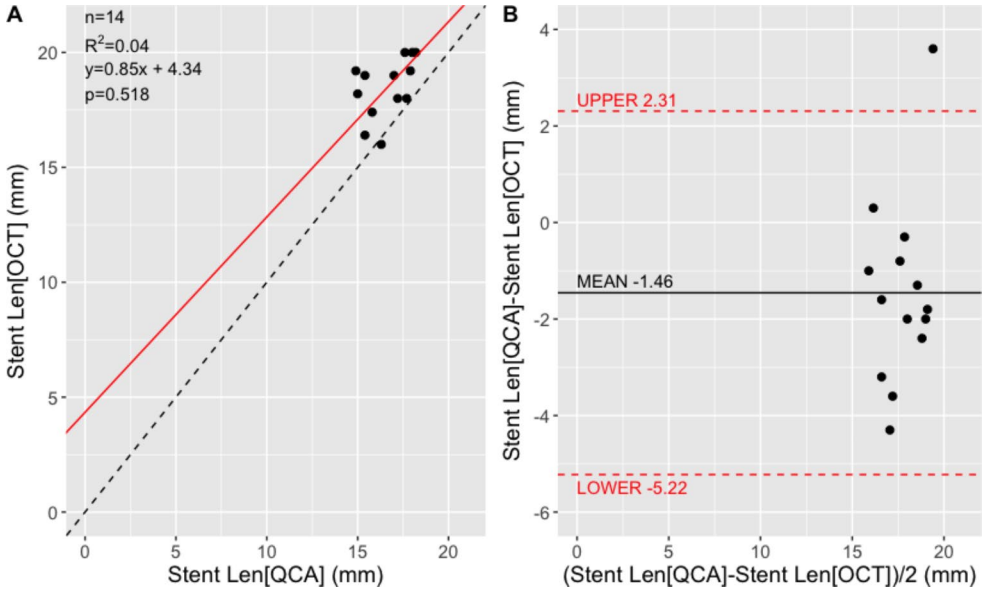

Fig. 5 Stent length measured from 3D-QCT and 3D-OCT fusion methods. **(A)** Passing and Bablok regression and **(B)** Bland-Altman analyses. Stent Len – stent length; QCA – quantitative coronary angiography; OCT – optical coherence tomography

Table 2 Linear and log-linear mixed effect linear regression. All axial coordinates have been standardised such that the scaffolded region covers the axial range [-0.5, 0.5] for every reconstruction

Model	Estimate type	Data used	Point Estimate	95% CI
Linear	Mean difference (ESS_{QCA} - ESS_{OCT}) [Pa]	All data available	1.37	(1.33, 1.41)
		Overlapping Sect. [1]	1.76	(1.72, 1.80)
		Restricted segment of interest[2]	1.51	(1.47, 1.55)
		Scaffolded segment only	1.97	(1.94, 2.00)
Log-linear	Ratio (ESS_{QCA} / ESS_{OCT}) [no units]	All data available	1.44	(1.44, 1.45)
		Overlapping Sect. [1]	1.52	(1.51, 1.52)
		Restricted segment of interest[2]	1.48	(1.47, 1.48)
		Scaffolded segment only	1.63	(1.62, 1.64)

[1] Including only ESS data where QCA and OCT sections are overlapping (according to standardised axial coordinates) for a given reconstruction of a given patient at a given time/visit

[2] Including only ESS data within 0.5 stent length of the distal or proximal end of the stent. That is, all data points with a standardised axial coordinate within the range [-1, 1]

restricted segment of interest, but this difference increased again for the scaffolded segment. In general, the shorter the segment around the stent one chooses to analyse the greater the expected difference between angiography-derived and OCT-derived ESS.

Figure 6 shows the ESS data as a function of the normalised axial coordinates. Each ESS data was modelled separately, with an additional spline function, for imaging modality and allowing for discontinuity in the ESS at the scaffolded segment boundary along the vessel (with axial position). The differences between angiography-derived and OCT-derived ESS varied according to axial location, in particular the differences between the 3 segments were notable. Overall, both scaffold and distal segment have a higher angiography-derived ESS than OCT-derived ESS. The opposite is true for the proximal segment.

Discussion

This study presents a comparison of angiography-derived *versus* OCT-derived ESS. Fourteen anatomically corrected 3D-QCA and 3D-OCT scaffolded artery models were reconstructed. ESS was derived from these models and was analysed simultaneously in both native and scaffolded segments. As with previous studies, our reconstructions demonstrated consistent underestimation of the MSA and scaffold length by 3D-QCA. While previous studies focusing on native coronary artery segments suggested good agreements between angiography-derived ESS *versus* IVUS or OCT-derived ESS [10–12], we have demonstrated 1.52 times higher ESS by 3D-QCA on the overlapping section (Table 2); 1.48 times over the restricted segment of interest. This discrepancy widens when considering only the scaffold segment. We have further demonstrated that this type of analysis and conclusion were highly sensitive to the ability to coregister the angiography-derived ESS to the OCT-derived ESS along the axial location beyond the scaffold's two metallic markers and other anatomical landmarks (Fig. 6), having displayed a cross-over in expected ESS in both proximal and distal native segment. A strong caveat but interesting at the same time. The all-important question here is in which vessel the ESS was measured – in the native coronary artery segment or in the scaffolded segment? And whether the prediction of micro-haemodynamic features is unique to

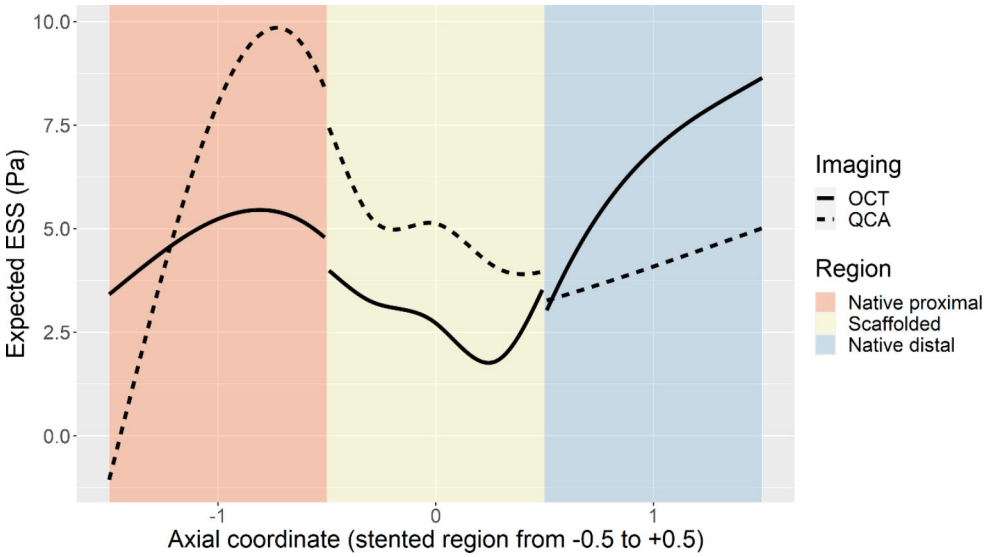

Fig. 6 Modelled ESS data along the vessel. ESS data were modelled as a function of axial coordinate with spline functions separately for imaging modality and segments

OCT-derived ESS? Interestingly, this will bring us back to the topics of imaging resolution and their impacts on a reliable reconstruction method between 3D-QCA, 3D-IVUS and 3D-OCT.

Impacts of an accurate arterial reconstruction

The accuracy of computational fluid dynamics (CFD) relies greatly on the reconstructed vessel anatomical models. Conventional coronary angiography has been considered the gold standard in coronary artery disease detection. This modality has been widely adopted by interventional cardiac catheterisation laboratories around the world [20]. Naturally, many clinicians and scientists favoured 3D arterial reconstructions using coronary angiography, such as 3D-QCA, for quantitative measurements and ESS investigations [i.e., angiography-derived ESS] [21]. On the other hand, advances in intravascular imaging (e.g., IVUS and OCT) offer clear delineation of the lumen and hence accurate lumen area measurements [22].

Lumen area (or diameter) represents one of the most critical factors in ESS calculations. According to Poiseuille flow analytical solution, ESS is proportional to mean blood flow inversely proportional to the lumen diameter (see Online Resource). With both coronary angiography and OCT being acquired in the same procedure, lumen diameter hence becomes the deciding factor. And due to the lack of contrast near the lumen surface in coronary angiography [3, 10], 3D-QCA tends to have a smaller lumen area than 3D-OCT or 3D-IVUS [mean difference − 2.38 mm^2] (Table 1; Fig. 4). The difference in lumen areas was one of the reasons for the higher angiography-derived ESS over the OCT-derived ESS (Table 2).

Another key difference in 3D arterial reconstruction using coronary angiography alone (3D-QCA) *versus* a fusion method (3D-OCT or 3D-IVUS) is that 3D-QCA assumes a circular or oval lumen from two end-diastolic projections and cannot accurately represent lumen irregularities [23]. On the other hand, the fusion approach replaces the circular or oval lumen borders with the actual lumen contours, accounting for local variation in geometry (Fig. 1). Local lumen irregularities could impact the development of blood flow distally, and create a unique response to distal shear stress pattern.

Lastly, there is a difference in arterial (stent) length between 3D-QCA and 3D-OCT. Foreshortening is a common effect of coronary angiography [24]. This underestimation might depend on the angle between the stent (artery) mid-plane and the imaging plane. Hence, 3D-QCA reconstruction reported a short stent length [mean difference − 1.46 mm] (Table 1; Fig. 5). In contrast, IVUS and OCT provide accurate axial measurements. IVUS's slower pullback speed allows for a more detailed scan along the artery in theory (i.e., IVUS has a higher axial resolution [~ 0.033 mm] than OCT [~ 0.1–0.2 mm]). However, IVUS fusion uses end-diastolic frames to match the 3D-centreline reconstructed coronary angiogram. This often means the IVUS frames used for reconstruction were more than 1 mm apart compared to OCT 0.1–0.2 mm axial resolution [25]. In addition, OCT offers a high radial resolution of 15 µm. The added axial and radial resolution for 3D-OCT has warranted a rethink of the current ESS analysis approach, particularly in segments where detailed 3D reconstruction, such as a scaffold [26, 27], plaque rupture or erosion [7, 8], endoluminal flap [9], etc., is essential to faithfully capture the local (or micro) haemodynamic environment and its subsequent impact to the distal flow environment.

Impacts of ESS analysis resolution

A detailed assessment of ESS also depends on the post CFD ESS analysis resolution. Previous studies often suggested

a 3 mm segment averaged analysis [28], or a 3 mm × 45º (60º or 90º) sector analysis [29]. Although a three-millimetre analysis demonstrated excellent correlations with plaque progression due to the macro plaque topology, 3 mm segment averaging might overlook the micro haemodynamic environments in CFD investigation involving both native and scaffold reconstructions. Given the sensitivity of ESS analysis along the axial location (as shown in Table 2), 3 mm segment averaging is best reserved for studies where the global health of the artery is of concern. A higher post CFD ESS analysing resolution (e.g., 0.1 mm) is needed in the presence of focal geometrical features, for example, stent struts, plaque rupture, erosion, dissection, etc.

Clinical implication

Our artery operates in a fine margin of ESS [30]. Outside this fine margin, low ESS was associated with lipid accumulation, up-regulation of inflammatory cytokines, and plaque progression [31–33]. On the other hand, high ESS were commonly associated with acute plaque rupture and erosion [7, 8]. While OCT-derived ESS might allow for an accurate ESS prediction and the finest detail analysis compared to angiography-derived ESS, OCT-derived ESS remains a multimodality, multi-step (Fig. 1) and time-consuming process as lumen delineation is a labour-intensive process. In addition, the finer the arterial geometry, the more computational grid points are needed, leading to a longer turnaround time in OCT-derived ESS. Hence, angiography-derived ESS remains the current go-to method today. However, there is a continuous research effort to reduce the turnaround time in OCT-derived ESS, including the use of artificial intelligence in the intravascular imaging delineation [34], and computational fluid dynamics [35]. OCT-derived ESS is expected to complement angiography-derived ESS in the near future. Hence, it is suggested to further deepen our understanding of the association between micro haemodynamic environment and disease progression and be ready for a point-of-care OCT-derived ESS analysis.

Limitations

This study has several limitations. First is the small sample size considered. Second is the limitation to a single type of scaffold. These limitations were related to the retrospective nature of the study that compared head-to-head the OCT-derived ESS from the original analysis [14]. However, it would be important to understand whether the differences in scaffold architecture, connector design, and strut geometry might affect the analysis. Thirdly, this study focused on imaging and post CFD ESS analysis resolutions, their associations with coronary artery disease and procedural outcomes have not been evaluated.

Conclusion

Angiography-derived ESS and OCT-derived ESS offer two distinctive methods of predicting coronary artery disease. Angiography-derived ESS tends to be higher than OCT-derived ESS due to the smaller lumen area. Imaging and post CFD ESS analysis resolutions play a vital role in OCT-derived ESS, and further studies are required.

Supplementary Information The online version contains supplementary material available at https://doi.org/10.1007/s10554-023-02949-0.

Acknowledgements This research was supported by the Research Computing Service NCI Access Scheme at The University of Melbourne.

Author contributions All authors contributed to the study's conception and design. Material preparation, data collection and analysis were performed by Eric Poon, Xinlei Wu and Neil O'Leary. The first draft of the manuscript was written by Eric Poon and all authors commented on previous versions of the manuscript. All authors read and approved the final manuscript.

Declarations

Competing interests Prof. Onuma reports institutional research grants related to his work as the chairman of cardiovascular imaging core labs of several clinical trials and registries sponsored by the industry, for which they receive no direct compensation. Prof. Serruys reports personal fees from Sino Medical Sciences Technology, Philips/Volcano, and Xeltis.

References

1. Dvir D, Marom H, Guetta V, Kornowski R (2005) Three-dimensional coronary reconstruction from routine single-plane coronary angiograms: in vivo quantitative validation. Int J Cardiovasc Intervent 7(3):141–145
2. Collet C, Onuma Y, Cavalcante R, Grundeken M, Genereux P, Popma J et al (2017) Quantitative angiography methods for bifurcation lesions: a consensus statement update from the european Bifurcation Club. EuroIntervention 13(1):115–123
3. Gutierrez-Chico JL, Serruys PW, Girasis C, Garg S, Onuma Y, Brugaletta S et al (2012) Quantitative multi-modality imaging analysis of a fully bioresorbable stent: a head-to-head comparison between QCA, IVUS and OCT. Int J Cardiovasc Imaging 28(3):467–478
4. Tu S, Holm NR, Koning G, Huang Z, Reiber JH (2011) Fusion of 3D QCA and IVUS/OCT. Int J Cardiovasc Imaging 27(2):197–207
5. Kilic Y, Safi H, Bajaj R, Serruys PW, Kitslaar P, Ramasamy A et al (2020) The evolution of Data Fusion Methodologies developed to reconstruct coronary artery geometry from intravascular imaging and coronary Angiography Data: a Comprehensive Review. Front Cardiovasc Med 7:33
6. Wu W, Khan B, Sharzehee M, Zhao S, Samant S, Watanabe Y et al (2021) Three dimensional reconstruction of coronary artery stents from optical coherence tomography: experimental validation and clinical feasibility. Sci Rep 11(1):12252
7. Yamamoto E, Thondapu V, Poon E, Sugiyama T, Fracassi F, Dijkstra J et al (2019) Endothelial shear stress and plaque Erosion: a

computational Fluid Dynamics and Optical Coherence Tomography Study. JACC Cardiovasc Imaging 12(2):374–375
8. Thondapu V, Mamon C, Poon EKW, Kurihara O, Kim HO, Russo M et al (2021) High spatial endothelial shear stress gradient independently predicts site of acute coronary plaque rupture and erosion. Cardiovasc Res 117(8):1974–1985
9. Poon EKW, Ono M, Wu X, Dijkstra J, Sato Y, Kutyna M et al (2023) An Optical Coherence Tomography and Endothelial Shear Stress Study of a Novel Bioresorbable Bypass Graft. Scientific Report. In press
10. Toutouzas K, Chatzizisis YS, Riga M, Giannopoulos A, Antoniadis AP, Tu S et al (2015) Accurate and reproducible reconstruction of coronary arteries and endothelial shear stress calculation using 3D OCT: comparative study to 3D IVUS and 3D QCA. Atherosclerosis 240(2):510–519
11. Bourantas CV, Ramasamy A, Karagiannis A, Sakellarios A, Zanchin T, Yamaji K et al (2019) Angiographic derived endothelial shear stress: a new predictor of atherosclerotic disease progression. Eur Heart J Cardiovasc Imaging 20(3):314–322
12. Naser J, Fogell N, Patel M, Yang P, Krams R, Wentzel JJ et al (2021) Moving shear stress towards the clinic: preclinical comparison of optical coherence tomography-based versus angiography-based time-averaged wall shear stress estimations. Eur Heart J 42
13. Serruys PW, Onuma Y, Ormiston JA, de Bruyne B, Regar E, Dudek D et al (2010) Evaluation of the second generation of a bioresorbable everolimus drug-eluting vascular scaffold for treatment of de novo coronary artery stenosis: six-month clinical and imaging outcomes. Circulation 122(22):2301–2312
14. Thondapu V, Tenekecioglu E, Poon EKW, Collet C, Torii R, Bourantas CV et al (2018) Endothelial shear stress 5 years after implantation of a coronary bioresorbable scaffold. Eur Heart J 39(18):1602–1609
15. Poon EKW, Thondapu V, Hayat U, Barlis P, Yap CY, Kuo PH et al (2018) Elevated blood viscosity and Microrecirculation resulting from Coronary Stent Malapposition. J Biomech Eng 140(5)
16. Kim HJ, Vignon-Clementel IE, Coogan JS, Figueroa CA, Jansen KE, Taylor CA (2010) Patient-specific modeling of blood flow and pressure in human coronary arteries. Ann Biomed Eng 38(10):3195–3209
17. Quemada D (1978) Rheology of Concentrated Disperse Systems.3. General features of the proposed non-newtonian model - comparison with experimental-data. Rheol Acta 17(6):643–653
18. Thondapu V, Shishikura D, Dijkstra J, Zhu SJ, Revalor E, Serruys PW et al (2022) Non-newtonian endothelial shear stress Simulation: does it Matter? Front Cardiovasc Med 9:835270
19. Bland JM, Altman DG (1986) Statistical methods for assessing agreement between two methods of clinical measurement. Lancet 1(8476):307–310
20. Garrone P, Biondi-Zoccai G, Salvetti I, Sina N, Sheiban I, Stella PR et al (2009) Quantitative coronary angiography in the current era: principles and applications. J Interv Cardiol 22(6):527–536
21. Bourantas CV, Zanchin T, Torii R, Serruys PW, Karagiannis A, Ramasamy A et al (2020) Shear stress estimated by quantitative coronary angiography predicts plaques prone to Progress and cause events. JACC Cardiovasc Imaging 13(10):2206–2219
22. Puri R, Tuzcu EM, Nissen SE, Nicholls SJ (2013) Exploring coronary atherosclerosis with intravascular imaging. Int J Cardiol 168(2):670–679
23. Tu S, Xu L, Ligthart J, Xu B, Witberg K, Sun Z et al (2012) In vivo comparison of arterial lumen dimensions assessed by co-registered three-dimensional (3D) quantitative coronary angiography, intravascular ultrasound and optical coherence tomography. Int J Cardiovasc Imaging 28(6):1315–1327
24. Green NE, Chen SY, Hansgen AR, Messenger JC, Groves BM, Carroll JD (2005) Angiographic views used for percutaneous coronary interventions: a three-dimensional analysis of physician-determined vs. computer-generated views. Catheter Cardiovasc Interv 64(4):451–459
25. Bourantas CV, Papafaklis MI, Lakkas L, Sakellarios A, Onuma Y, Zhang YJ et al (2014) Fusion of optical coherence tomographic and angiographic data for more accurate evaluation of the endothelial shear stress patterns and neointimal distribution after bioresorbable scaffold implantation: comparison with intravascular ultrasound-derived reconstructions. Int J Cardiovasc Imaging 30(3):485–494
26. O'Brien CC, Kolandaivelu K, Brown J, Lopes AC, Kunio M, Kolachalama VB et al (2016) Constraining OCT with knowledge of device design enables high accuracy hemodynamic Assessment of Endovascular Implants. PLoS ONE 11(2):e0149178
27. Tenekecioglu E, Poon EKW, Collet C, Thondapu V, Torii R, Bourantas CV et al (2016) The Nidus for possible Thrombus formation: insight from the Microenvironment of Bioresorbable Vascular Scaffold. JACC Cardiovasc Interv 9(20):2167–2168
28. Stone PH, Saito S, Takahashi S, Makita Y, Nakamura S, Kawasaki T et al (2012) Prediction of progression of coronary artery disease and clinical outcomes using vascular profiling of endothelial shear stress and arterial plaque characteristics: the PREDICTION Study. Circulation 126(2):172–181
29. Mazzi V, De Nisco G, Hoogendoorn A, Calo K, Chiastra C, Gallo D et al (2021) Early atherosclerotic changes in coronary arteries are Associated with Endothelium Shear stress Contraction/Expansion variability. Ann Biomed Eng 49(9):2606–2621
30. Wentzel JJ, Janssen E, Vos J, Schuurbiers JC, Krams R, Serruys PW et al (2003) Extension of increased atherosclerotic wall thickness into high shear stress regions is associated with loss of compensatory remodeling. Circulation 108(1):17–23
31. Bourantas CV, Zanchin T, Sakellarios A, Karagiannis A, Ramasamy A, Yamaji K et al (2019) Implications of the local haemodynamic forces on the phenotype of coronary plaques. Heart 105(14):1078–1086
32. Yamamoto E, Siasos G, Zaromytidou M, Coskun AU, Xing L, Bryniarski K et al (2017) Low endothelial shear stress predicts evolution to high-risk coronary plaque phenotype in the future: a serial optical coherence tomography and computational Fluid Dynamics Study. Circ Cardiovasc Interv 10(8)
33. Vergallo R, Papafaklis MI, Yonetsu T, Bourantas CV, Andreou I, Wang Z et al (2014) Endothelial shear stress and coronary plaque characteristics in humans: combined frequency-domain optical coherence tomography and computational fluid dynamics study. Circ Cardiovasc Imaging 7(6):905–911
34. Bajaj R, Huang X, Kilic Y, Ramasamy A, Jain A, Ozkor M et al (2021) Advanced deep learning methodology for accurate, real-time segmentation of high-resolution intravascular ultrasound images. Int J Cardiol 339:185–191
35. Gharleghi R, Samarasinghe G, Sowmya A, Beier S (2020) 377 machine learning to predict hemodynamic risk in Left Main Bifurcations. Heart Lung and Circulation 29:S207
36. Gijsen F, Katagiri Y, Barlis P, Bourantas C, Collet C, Coskun U et al (2019) Expert recommendations on the assessment of wall shear stress in human coronary arteries: existing methodologies, technical considerations, and clinical applications. Eur Heart J 40(41):3421–3433